NOTES AND CORRESPONDENCE

On Quasigeostrophic Normal Modes in Ocean Models: Weakly Nonseparable Situation

UWE HARLANDER AND LEO R. M. MAAS

Netherlands Institute for Sea Research, Texel, Netherlands

30 January 2003 and 30 March 2004

ABSTRACT

This study examines quasigeostrophic Rossby eigenmodes of homogeneous as well as stratified oceans. Analytical studies of Rossby basin modes are usually done by using simple basin geometries. Simple means that solutions are available by applying a separation *ansatz* in looking for basin modes. Here the focus is on half-trapezoidal geometry, in particular on a stratified ocean with a half-trapezoidal (zonal) cross section. In this case, separation is not possible. However, approximate solutions can be found. Different approximations are discussed: one related to linearization of the boundary conditions, one related to a sight change in boundary geometry, and one that uses an asymptotic expansion. It is shown that the widely used ''linearized boundary conditions'' give wrong results for low-frequency modes. The reason is that weak asymmetries of the basin are neglected and wave energy is therefore distributed too homogeneously in the basin. Although the basin's geometry used deviates only slightly from a square and the eigenvalue spectrum corresponds well with that of a square basin, eigenmodes can still differ greatly.

1. Introduction

An important problem in geophysical fluid dynamics is the study of the eigenvalue spectra and the eigenmodes for large-scale models of atmospheres and oceans. In general, this examination is done numerically—for example, by finite differences (Holland 1978), finite elements (Platzman 1978), or spectral methods (Sheremet et al. 1997). The reasons for doing so can be complicated basin boundaries, simple boundaries but a complicated model, or complicated boundaries and model both. All numerical techniques, though powerful, have limitations. For example, a large number of ''numerical experiments'' are necessary to test the effect of parameter changes on the solutions. In contrast, analytical solutions give a complete description that helps one to understand the nature of modes found numerically and that can be used to test numerical schemes. Therefore it is still important to complete our knowledge on analytical solutions of models of geophysical fluid dynamics.

Free quasigeostrophic Rossby modes, relevant in oceanography, have been investigated analytically for different boundary geometries and flow conditions—for example, fluids at rest in closed basins (Flierl 1977; Pedlosky 1987) and jet flows along coastlines (Harlander et al. 2000, 2001). Special geometries have been chosen to keep the problems tractable analytically. LeBlond and Mysak (1978) and Pedlosky (1987) discuss rectangular basins, and Flierl (1977) has solved the problem for circular geometry; an isosceles right triangle (Polyanin 2002) or an equilateral triangle (McCartin 2003) would also be suitable, that is, would also give a separable equation. Here we focus on a weakly nonseparable problem by using a nearly rectangular basin (see Fig. 1). We consider two-dimensional barotropic and baroclinic situations.

Our interest lies in the effects of small changes in basin geometry on the eigenmodes of the classical Helmholtz equation with homogeneous Dirichlet boundary conditions. Therefore, the barotropic model version describes solutions corresponding to $R \gtrsim L$, where R is the deformation radius and L is the basin length scale (McWilliams 1977; Flierl 1977). [For quasigeostrophic reduced gravity models $R \ll L$ holds. In that case the model equation can be transformed to a nonhomogeneous Helmholtz equation with homogeneous Dirichlet boundary conditions (LaCasce and Pedlosky 2002). Note that for this case the solutions of the homogeneous problem are still important, because they are needed to construct solutions for the full problem (see Polyanin 2002, p. 492).] On the other hand, with the baroclinic situation mentioned above, we mean a continuously stratified fluid enclosed in an infinite, north–south-oriented open channel with a half-trapezoidal cross section

Corresponding author address: Uwe Harlander, The Netherlands Institute for Sea Research, P.O. Box 59, 1790 AB Texel, Netherlands. E-mail: harland@nioz.nl

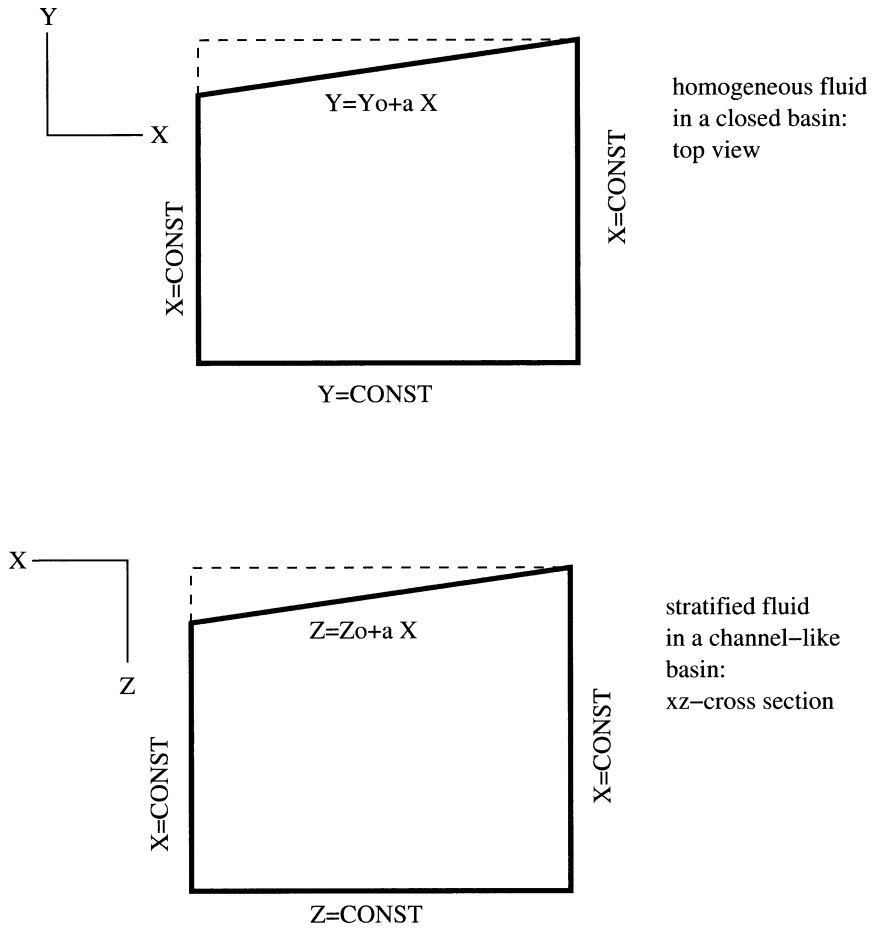

FIG. 1. Basin geometry for the (top) barotropic and (bottom) baroclinic situations discussed in the text: x corresponds to the zonal direction, y corresponds to the meridional direction, and z corresponds to the vertical direction. In the lower part of the figure, we assume that the lateral sidewalls deviate from being strictly vertical.

(see Fig. 1, bottom). In section 2 it will be shown that this model too can be reduced to the Helmholtz equation and that- homogeneous Dirichlet boundary conditions are appropriate. After that, we continue by discussing eigensolutions of the classical Helmholtz problem for the half-trapezoidal domain obtained by using different approximations. For simplicity, we restrict the study to dimension two; that is, we neglect meridional variation in the baroclinic 3D model. First, we consider the so-called linearized boundary condition in which, for example, $w[t, x, h(x)] = uh_x$ is replaced by $w(t, x, h_0) = uh_x$, where u is horizontal velocity, w is vertical velocity, h is bottom topography, and h_0 is mean depth (Rhines 1970; Pedlosky 1987; Straub 1994). Second, we slightly deform the basin's boundary to a certain disk segment to get a separable problem. Last, we use an asymptotic form of the equation but for the actual boundary shape. We address the following questions: how does modification of the basin's geometry affect 1) the spectrum of the eigenvalues and 2) the shape (or ''dressing'') of the eigenmodes? We will show that the widely used ''linearized boundary condition'' leads to wrong low-frequency modes, even for small boundary slopes. An important question related to ocean eigenmodes is whether those modes fulfill additional integral constraints of the flow. We will discuss this point for both models (see sections 2 and 3).

The paper is organized as follows. In section 2, we describe how to derive the Helmholtz equation for the barotropic and baroclinic cases considered. We investigate also under which conditions integral constraints are not violated. In section 3, we study different solutions corresponding to different approximations. Last, in section 4 we discuss our results and end with a brief conclusion.

2. Model

a. Barotropic situation

Let us first focus upon the linearized barotropic quasigeostrophic potential vorticity equation on the β-plane (Pedlosky 1987, p. 144),

$$\frac{\partial}{\partial t}[\nabla^2\psi(x, y, t) - F\psi(x, y, t)] + \beta\frac{\partial\psi(x, y, t)}{\partial x} = 0, \quad (1)$$

where ψ is the geostrophic streamfunction, $\boldsymbol{\nabla} = (\partial/\partial x, \partial/\partial y)$is the two-dimensional nabla operator (x denotes zonal direction and y is meridional direction), β is a constant related to the beta-plane assumption, and $F = f_0^2L^2/gD$, with f_0 being Coriolis parameter, L being length scale, g being constant of gravity, and D being mean ocean depth. Using $\psi = \hat{\psi}(x, y)\exp\{-i[(x/2\omega) + (\omega\beta t)]\}$, where ω denotes frequency, we obtain the Helmholtz equation

$$\nabla^2\hat{\psi}(x, y) + \hat{K}^2\hat{\psi}(x, y) = 0, \quad (2)$$

with $\hat{K}^2 = (1/4\omega^2) - F$. At the boundary $\mathcal{D}$ generally $\psi(x, y, t) = \Gamma(t)$ is applied. Then $\Gamma(t)$ is determined such that mass conservation,

$$\frac{\partial}{\partial t}\int_{\mathcal{A}}\frac{g}{f_0}h_s\, dx\, dy = \frac{\partial}{\partial t}\int_{\mathcal{A}}\psi\, dx\, dy = 0, \quad (3)$$

is fulfilled, where $\mathcal{A}$ is the model domain and h_s is the relative height of the free surface, related to ψ through the geostrophic balance. However, Flierl (1977) showed that for moderate values of F a homogeneous Dirichlet boundary condition, $\hat{\psi}(x, y) = 0$ at $\mathcal{D}$, is appropriate also. In such a model we have typically $L \lesssim R$, where L denotes the basin scale and R is the Rossby deformation radius. [The situation $F = 0$ corresponds to a rigid-lid assumption when deriving (1).] As mentioned in the introduction, $F \gg 1$ has been used in recent studies of quasigeostrophic thermocline dynamics. However, it should be noted that F actually must be at most order 1 to be consistent with the barotropic quasigeostrophic model. This model is derived through a perturbation analysis using the small Rossby number as perturbation parameter (Pedlosky 1987). A model parameter larger than order 1 affects the analysis and would lead to a different model. For large F, a planetary geostrophic model should be more suitable to describe Rossby wave dynamics than a quasigeostrophic model is.

It is worth mentioning that Gerdes and Wübber (1991) have used homogeneous Dirichlet boundary conditions $\psi = 0$ instead of the exact condition $\psi = \Gamma(t)$ in their 3D quasigeostrophic numerical model of the North Atlantic Ocean. They argue that, for ocean basins that are open at the northern and southern side, homogeneous Dirichlet boundary conditions avoid the occurrence of unrealistic oscillating boundary currents, leading to an eddy potential energy that is 3 times that in a corresponding primitive equation model. Viewed in this light, even if $F > 1$, homogeneous Dirichlet boundary conditions might be a proper choice for quasigeostrophic models of semiclosed ocean basins.

Note further that the basin shown in the top panel of Fig. 1 can be rotated to any angle γ without changing the solutions of (2). However, the first part of the carrier wave then reads

$$\exp[-i(x\cos\gamma - y\sin\gamma)/2\omega], \quad (4)$$

and therefore (3) depends on γ. In the following we are interested in solutions of (2), that fulfill homogeneous Dirichlet boundary conditions, as well as (3). It should be mentioned that for more general settings, for example, with a small Rossby deformation radius and related time-dependent boundary conditions, the modes, as well as the constraints, depend on γ (LaCasce and Pedlosky 2002).

b. Baroclinic situation

The Helmholtz equation with homogeneous boundary conditions is important also in the baroclinic case as we show in the following. The baroclinic quasigeostrophic model linearized about a state of rest (see Pedlosky 1987, p. 375) is

$$\frac{\partial}{\partial t}\left[S^{-1}\frac{\partial^2\psi}{\partial z^2} - (SH)^{-1}\frac{\partial\psi}{\partial z} + \nabla_h^2\psi\right] + \beta\frac{\partial\psi}{\partial x} = 0, \quad (5)$$

where H is a constant-density scale height, $S = (N^2D^2)/(f_0^2L^2)$, $\beta = (\beta_0Lf_0)/U$, and N, L, D, U, ρ_0, f_0, and β_0 are dimensional constants. They stand for Brunt–Väisälä frequency, length scale, fluid thickness scale, velocity scale, mean density, Coriolis parameter, and beta-plane parameter, respectively. As lateral and vertical boundary conditions,

$$(u, v)\cdot\mathbf{n} = 0 \quad \text{and} \quad (6)$$

$$w(z = h) = J[\psi, h(x, y)] \quad (7)$$

are generally used, where $J(A, B) = \partial A/\partial x\,\partial B/\partial y - \partial A/\partial y\,\partial B/\partial x$, (u, v, w) are the velocity components, h is topography, and $\mathbf{n}$ is the unit normal vector perpendicular to the walls. The streamfunction ψ is related to the velocity components as

$$u = -\frac{\partial\psi}{\partial y}, \qquad v = \frac{\partial\psi}{\partial x}, \quad \text{and} \quad w = -\frac{1}{S}\frac{\partial^2\psi}{\partial t\partial z}. \quad (8)$$

Using $(x, y) = 2S^{1/2}(x', y')$, $z = 2z'$, and $t = (2S^{1/2}\beta)^{-1}t'$, we transform (5) to

$$\frac{\partial}{\partial t'}\left(\nabla'^2\psi - \frac{2}{H}\frac{\partial\psi}{\partial z'}\right) + \frac{\partial\psi}{\partial x'} = 0, \quad (9)$$

where $\boldsymbol{\nabla}' = (\partial/\partial x', \partial/\partial y', \partial/\partial z')$. Further,

$$u = -(2S^{1/2})^{-1}\frac{\partial\psi}{\partial y'}, \qquad v = (2S^{1/2})^{-1}\frac{\partial\psi}{\partial x'}, \quad \text{and}$$

$$w = -\beta S^{-1/2}\frac{\partial^2\psi}{\partial t'\partial z'}. \quad (10)$$

In terms of the vertical velocity, (9) reads as

$$\frac{\partial}{\partial t'}\left(\nabla'^2w - \frac{2}{H}\frac{\partial w}{\partial z'}\right) + \frac{\partial w}{\partial x'} = 0. \quad (11)$$

Let us now assume symmetry in the meridional direc-

tion; that is, all meridional derivatives vanish.[1] Then ∇' simplifies to $\nabla' = (\partial/\partial x', \partial/\partial z')$. The continuity equation connecting the vertical velocity to the ageostrophic horizontal motion reads for a flow independent of y' as

$$S^{-1/2}\frac{\partial u_a}{\partial x'} + \frac{\partial w}{\partial z'} = 0. \tag{12}$$

In addition to ψ we can now introduce an ageostrophic streamfunction χ:

$$u_a = -S^{1/2}\frac{\partial \chi}{\partial z'} \quad \text{and} \quad w = \frac{\partial \chi}{\partial x'}. \tag{13}$$

In the following we drop the primes. Using the transformation (LeBlond and Mysak 1978)

$$\chi = \hat{\chi}(x, z)\Lambda(x, z, t), \quad \text{where } \Lambda(x, z, t) = \exp\left[\frac{z}{H} - i\left(\frac{x}{2\omega} + \omega t\right)\right], \tag{14}$$

(to remove the first-order derivatives), we obtain from (11), (13), and (14):

$$\frac{\partial}{\partial x}[\Lambda(x, z, t)(\nabla^2\hat{\chi} + K^2\hat{\chi})] = 0, \tag{15}$$

where $K^2 = 1/(4\omega^2) - 1/H^2$. The boundary conditions for an arbitrary xz cross section read $(u_a, w)\cdot\mathbf{n} = 0$; that is; $\chi = \Gamma(t)$along the boundary. Here $\Gamma(t)$ can be found from mass conservation. This constraint reads for the baroclinic quasigeostrophic model as

$$\frac{1}{S}\frac{\partial}{\partial t}\int_{\mathcal{V}} \rho\, dx\, dz\, dy = \int_{-\infty}^{\infty}\left(\int_{\mathcal{A}} w\, dx\, dz\right) dy = 0, \tag{16}$$

where $\mathcal{V}$ and $\mathcal{A}$ are volume and area (of the xz cross section) covered by the basin. To obtain (16) we used the fact that in quasigeostrophic flows the vertical velocity w [see (8)] as well as the density $\rho = -\partial\psi/\partial z$ can be computed from the geostrophic streamfunction ψ. If we introduce χ into (16) we obtain

$$\int_{\mathcal{A}} w\, dx\, dz = \int_{\mathcal{A}} \frac{\partial \chi}{\partial x}\, dx\, dz = \int [\chi(b, z, t) - \chi(a, z, t)]\, dz = 0, \tag{17}$$

because $\chi(b, z, t) = \chi(a, z, t) = \Gamma(t)$, where $x = a$ and b are the locations of the two lateral boundaries. It is obvious that (16) is fulfilled for any choice of $\Gamma(t)$. Without loss of generality we assume $\Gamma(t) = 0$.

We find that for a y independent flow, the solution of (5) can be obtained by solving

$$\nabla^2\hat{\chi} + K^2\hat{\chi} = 0, \tag{18}$$

with

$$\hat{\chi} = 0 \text{ at } \mathcal{D},$$

in full analogy to the barotropic situation.

Equations (2) and (18) correspond to the classical Helmholtz equations with homogeneous Dirichlet boundary conditions. This equation can be found in many fields of mathematical physics, for example, as the harmonic acoustic wave equation, the harmonic Maxwell equation, and the harmonic elastic wave equation (Nedelec 2001). It plays a dominant role also in the field of water surface waves and quantum mechanics (Stöckmann 1999).

3. Results

Let us consider an almost rectangular domain shown in Fig. 1. This is either an ocean basin filled with a barotropic fluid seen from above or the zonal xz cross section of a channel-like ocean filled with a stratified fluid. In the first case, the northern coastline is not purely zonal; in the second situation, we consider a basin with bottom topography. However, as said before, with the restrictions made, both situations are mathematically equivalent; that is, both cases are treated when (18) is solved.

a. Solving (18) by simplifying the lower boundary condition

We assume that the sloping boundary is given by $h = h_0 + \alpha x$, where h_0 as well as $\alpha \ll 1$ are constants. The vertical velocity w can be expanded in a Taylor series around the mean depth h_0,

$$w(t, x, z) = w(t, x, h_0) + \frac{\partial w}{\partial z}|_{z=h_0}(z - h_0) + \cdots \tag{19}$$

Arguing that for $z \approx h$, w as well as $z - h_0$ are $O(\alpha)$, we obtain to order α: $w(t, x, h) \approx w(t, x, h_0)$. For small slopes, (7) is therefore simplified by assuming

$$w(z = h_0) = J[\psi, h(x)]; \tag{20}$$

that is,

$$\hat{\chi} = 0 \text{ at } \mathcal{D}_0 \tag{21}$$

in (18), where $\mathcal{D}_0$ corresponds to the (dashed) *rectangle* shown in Fig. 1 and not to the original half-trapezoidal geometry.

This assumption is usually considered to be consistent with the quasigeostrophic assumption (Rhines 1970) and is applied in many conceptual studies (Pedlosky 1987; Straub 1994). However, using this simplification the originally nonseparable problem turns separable, and this might be the reason why that approximation can be found so frequently in theoretical studies. Note that the

[1] Note that in this case the nonlinear term in the quasigeostrophic model vanishes; that is, the solutions presented are also valid for the nonlinear model.

same arguments hold for the barotropic situation by replacing w and z_0 by v and y_0.

Let us assume a box bounded by $x = 0$ and π in the horizontal direction and bounded in the vertical direction by $z = 0$ and π. Applying (20), we use the separation *ansatz* $\hat{\chi} = \phi(x)\sin nz$, $n \in \mathbb{N}$, which fulfills the approximated top/bottom boundary condition. It remains

$$\phi_{xx} + \hat{k}^2\phi = 0, \tag{22}$$

where $\hat{k}^2 = K^2 - n^2$. We find $\phi = A\cos\hat{k}x + B\sin\hat{k}x$. Last, by applying the boundary conditions, we get $A = 0$ and $\hat{k} = k \in \mathbb{N}$. To summarize the findings,

$$\hat{\chi} = B\sin kx\sin nz, \qquad k \in \mathbb{N}, \qquad n \in \mathbb{N}, \quad \text{and} \tag{23}$$

$$K^2 = \frac{1}{4\omega^2} - \frac{1}{H^2} = k^2 + n^2. \tag{24}$$

Note that although the baroclinic model is mass conserving, this constraint holds in the barotropic situation for even meridional wavenumbers only.

b. Solving (18) by deforming the lateral boundaries

Converting (18) to polar coordinates (r, θ), we get

$$\hat{\chi}_{rr} + \frac{1}{r}\hat{\chi}_r + \frac{1}{r^2}\hat{\chi}_{\theta\theta} + K^2\hat{\chi} = 0. \tag{25}$$

In the following we solve this equation not for the asymmetric box shown in Fig. 1, but for a segment of a wedge with an angle μ. The upper surface is considered horizontal, whereas the slope of the bottom is determined by μ. In the lateral direction the segment is bounded by two circles with radii r_1 and r_2. With the assumption that $r_2 - r_1 = \pi$ and that the arclength $r_2\mu = \pi$, r_1 and r_2 are determined by the slope μ.

It is obvious that the lateral sidewalls are curved now, in contrast to the lateral walls in Fig. 1; however, for $\mu \to 0$, the segment under consideration converges to the box considered in section 3a. The purpose is to compare modal solutions in the segment for small μ (large r_2) with the solutions given in section 3a (see section 4). Picking $\hat{\chi} = \phi\sin(n\pi\theta/\mu)$ with $n \in \mathbb{N}$ (which fulfills the top/bottom boundary conditions), we obtain

$$\phi_{r'r'} + \frac{1}{r'}\phi_{r'} + \left[1 - \left(\frac{n\pi}{\mu r'}\right)^2\right]\phi = 0, \tag{26}$$

where $r' = Kr$. This is Bessel's equation with the general solution

$$\phi = AJ_\nu(Kr) + BY_\nu(Kr), \tag{27}$$

where $\nu = (n\pi)/\mu$. The function $J_\nu(Y_\nu)$ is called Bessel function of the first (second) kind (Abramowitz and Stegun 1965). Using the lateral boundary conditions, K follows from

$$J_\nu(Kr_1)Y_\nu(Kr_2) - J_\nu(Kr_2)Y_\nu(Kr_1) = 0, \tag{28}$$

and the solution is determined, up to a constant A, as

$$B = -[J_\nu(Kr_1)/Y_\nu(Kr_1)]A. \tag{29}$$

Note that, in the barotropic situation, (16) is fulfilled if the basin is symmetric with respect to the zonal direction (i.e., $\theta \in [-\mu, \mu]$). We will discuss differences of solution (27) and (23) in section 4 and will point out the physical meaning of their discrepancy for oceanic Rossby waves.

c. Solving (18) by simplifying the equation

Let us consider that the upper and lower boundaries for (18) are given by $z = 0, -G(\epsilon^2 x)$. We require $\epsilon \ll 1$. In making the *ansatz*

$$\hat{\chi} = \phi(x)\sin\{\hat{n}(x)[z + G(x)]\}, \tag{30}$$

the vertical boundary conditions are fulfilled if

$$\hat{n}(x) = \frac{n\pi}{G(x)} \tag{31}$$

with

$$n \in \mathbb{N}.$$

To order ϵ we find

$$\epsilon^2\phi_{XX} - q\phi = 0, \tag{32}$$

where $q = \hat{n}^2 - K^2$ and $X = \epsilon x$. For general G, this equation can be solved by using the Wentzel–Kramers–Brillouin approximation. However, assuming that G is a linear function of x, an analytical solution of (32) exists.

We consider $G = \pi + \alpha x$, with lateral walls at $x = 0$ and $-\pi$, and $\epsilon^2 = \alpha = \tan\mu$. We obtain

$$\phi(x) = AG^{1/2}J_\nu(KG/\alpha) + BG^{1/2}Y_\nu(KG/\alpha), \tag{33}$$

with $\nu = \sqrt{\alpha^2 + n^2\pi^2}/(2\alpha)$ and the boundary conditions $\phi(-\pi) = \phi(0) = 0$. The eigenvalue K and A, B can be found by applying (28) and (29).

The eigenvalue spectrum can be computed more easily if we use

$$\hat{n}^2 = \left(\frac{n\pi}{\pi + \alpha x}\right)^2 \approx n^2\left(1 - \frac{2\alpha}{\pi}x\right), \tag{34}$$

which is a good approximation if α is small (Zaitsev et al. 2001). In that case we obtain

$$\phi(x') = A\mathrm{Ai}(-K'^2 - x') + B\mathrm{Bi}(-K'^2 - x'), \tag{35}$$

where Ai and Bi are the Airy functions (Abramowitz and Stegun 1965), $x' = \tilde{\alpha}x$, $\tilde{\alpha} = (n^2\alpha/2\pi)^{1/3}$, and $K' = (K^2 - n^2/4)/\tilde{\alpha}^2$. The eigenvalues K' are given by

$$\mathrm{Ai}(-K'^2 + \tilde{\alpha}\pi)\mathrm{Bi}(-K'^2) - \mathrm{Bi}(-K'^2 + \tilde{\alpha}\pi)\mathrm{Ai}(-K'^2) = 0. \tag{36}$$

TABLE 1. Eigenvalues for different modes (i.e., different κ) and different vertical wavenumbers n. Here $\mu = 0.1$ and $H = F = 1$.

Solution	κ	n	K	k	ω
(27)	2	1	2.2602	—	0.2022
(33)	2	1	2.2608	—	0.2022
(23)	2	1	2.2361	2	0.2041
(35)	2	1	2.2584	—	0.2024
(27)	3	4	5.1769	—	0.0948
(33)	3	4	5.1776	—	0.0948
(23)	3	4	5.0000	3	0.0980
(35)	3	4	5.1599	—	0.0951
(27)	1	9	9.3927	—	0.0529
(33)	1	9	9.3936	—	0.0529
(23)	1	9	9.0554	1	0.0549
(23)	3	9	9.4868	3	0.0524
(35)	1	9	9.3806	—	0.0530
(27)	2	9	9.6953	—	0.0513
(33)	2	9	9.6969	—	0.0513
(23)	2	9	9.2195	2	0.0539
(23)	4	9	9.8488	4	0.0505
(35)	2	9	9.6599	—	0.0515

4. Discussion and conclusions

We now want to compare solutions (27), (33), and (35), which take the slope in geometry into account, with (23), which actually does not. First we specify the slope μ and the vertical wavenumber n. Second, we compute the corresponding eigenvalue K and the related eigenmode by using (27), (33), or (35). Then we can proceed in two ways: either we compare modes directly—that is, solutions with the same number of nodes in the vertical and horizontal directions but with possibly different frequencies (method 1)—or we choose k in (24) such that the frequencies correspond best and accept that the number of crests and troughs in the horizontal direction, κ, might differ (method 2).

Table 1 shows some eigenvalues K for different κ and different choices of vertical wavenumber n. It can be seen that, using method 2, the eigenvalues K (and frequencies) are similar when the approximate solutions (27), (33), (35), or (23) are employed. Using method 1, eigenvalues differ when n increases.

The important thing is that, no matter which comparison method is used, the eigenfunctions corresponding to (27), (33), or (35) differ from (23) when n increases. When the linearized boundary condition from section 3a is applied, the corresponding eigensolutions are always symmetric in both spatial directions. This holds only for small vertical wavenumbers n in (27), (33), or (35). As demonstration we plotted mode 2, with $n = 1$ in Fig. 2 [Fig. 2a corresponds to (33), and Fig. 2b corresponds to (23)], and mode 1, with $n = 9$ in Fig. 3 [Fig. 3a corresponds to to (33), and Fig. 3b corresponds to (23) by using comparison method 1]. We find that (i) eigensolutions agree well when approximations (27) and (33) are used (not shown) and (ii) left-right symmetry breaking is not captured when (23) is applied. Note that symmetry is lost although the condition $n \ll 2\pi/(\alpha L)$ is not violated; even with $n = 9$ we still handle solutions that are usually considered consistent with the linearized boundary condition discussed in section 3a. Fig. 3 shows that an amplitude maximum establishes itself in the deep part of the domain and the zonal wavelength increases toward the shallow region. The mode seems to be trapped at the right wall, that is, no energy can reach the shallow part of the basin.

Figure 4 shows the first nine eigenvalues K computed from (36) (crosses) and from (23) (circles) using $n = 1$ (lower curve), $n = 4$ (middle curve), and $n = 9$ (upper curve). For small vertical wavenumbers n the eigenvalues K are virtually the same, but even for large wavenumbers the relative difference is small (see also Table 1). In contrast, the eigenfunctions can become very different as can be seen by comparing Fig. 3a with Fig. 3b. Note that the approximation (34) does not affect the solution, as can be seen by comparing it with (23) and (33). Note further that, for a given n, the most significant asymmetry occurs for the first modes (low number of eigenvalue in Fig. 4) and not for the very low frequency modes.

What can be learned from this study? First, we found that it can be dangerous to use the linearized boundary condition. The reason is that even weak asymmetry can have a prominent effect on higher modes; for example, boundary trapped waves can be found, but only when the exact and not the linearized boundary conditions are applied. Second, breaking the symmetry of the basin removes degeneracy from the eigenvalue spectrum (see Fig. 4), which opens the possibility for *beat phenomena* with long time scales (see discussion below). Last but not least, the model we presented (a 2D baroclinic model formulated in terms of ageostrophic vertical streamfunction instead of geostrophic horizontal streamfunction) appears to be new.

The first two points are maybe the most important ones from an oceanographic point of view, and we will discuss them in greater detail in the following. From (23) and (24) we see that, for the box-shaped symmetric basin, different eigenfunctions can correspond to the same eigenvalue, e.g., $n = 1$ and $k = 4$ give the same K as $n = 4$ and $k = 1$ do. Such spectra are called degenerate. In contrast, the degeneracy is removed when the domain with the sloping wall is considered (see also Fig. 4). However, if the symmetry is weakly broken, the former degenerate eigenvalues are close together in the nondegenerate spectrum. Therefore the corresponding eigenmodes will usually be excited together, giving rise to beat phenomena. This condition means that, even when the eigenfrequencies of such modes are large in comparison with climate time scales, the beat oscillation can introduce low-frequency variability. We think that such almost degenerate basin modes should be taken into account in studies of interannual to interdecadal variability signals.

Let us now turn to the first point mentioned above. As we have seen, low-frequency modes can look very different for symmetric or slightly nonsymmetric basins,

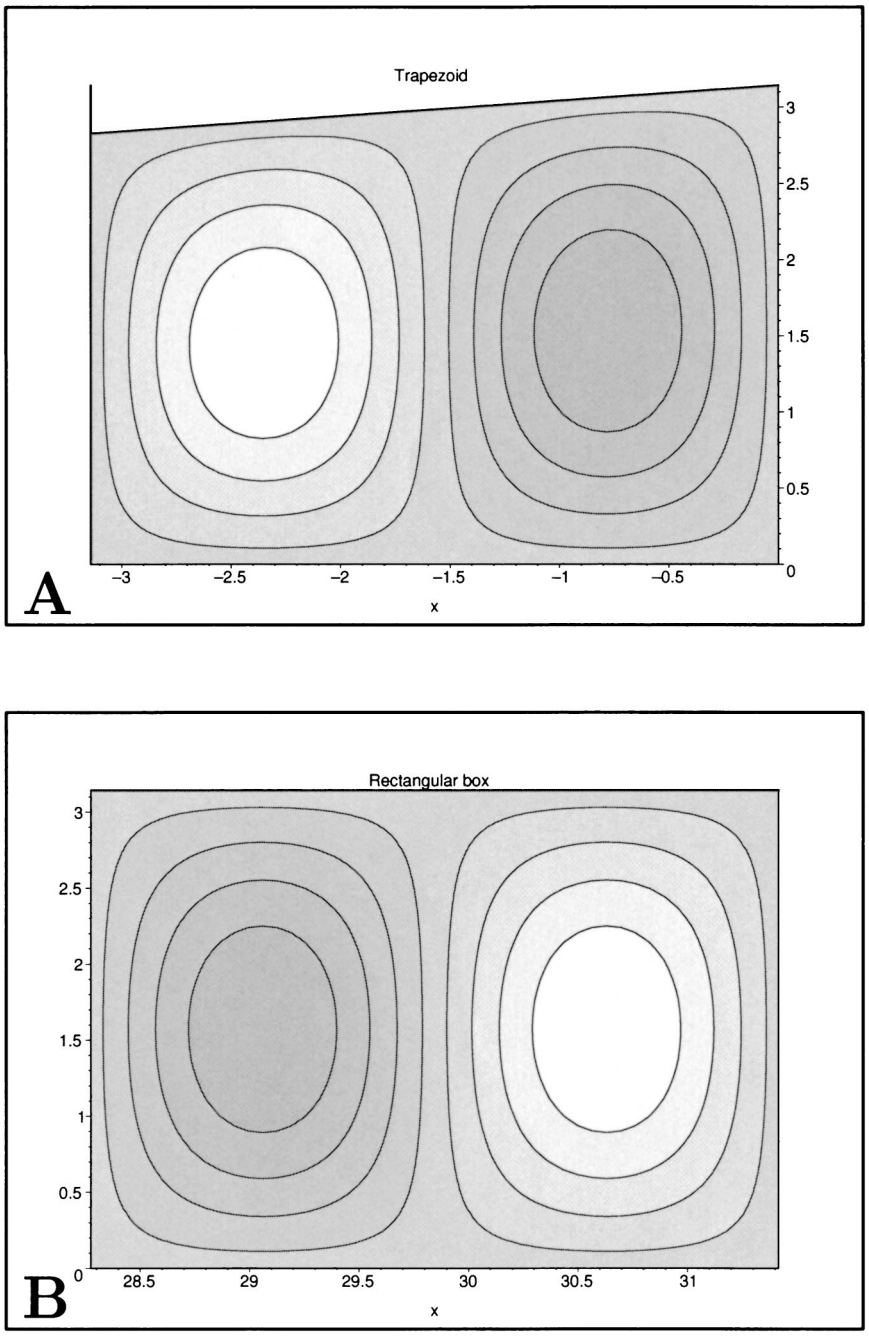

FIG. 2. Mode-2 solution of (a) (33) and (b) (23). Vertical wavenumber is $n = 1$, $\mu = 0.1$.

even for small slopes. In physical terms, the symmetry breaking can be understood in terms of wave energy propagation. Energy ray steepening for upslope propagating waves is a well-known effect in acoustics (Jensen et al. 2000). For larger vertical wavenumbers, the rays of the Rossby wave group velocity have a large tilt with respect to the zonal direction. If such waves propagate upslope, they experience multiple reflections at the sloping surface, which leads to a steepening of the group velocity vectors. If the number of reflections is sufficient, the rays show turning points before reaching the wall located at the shallow part of the basin. This phenomenon explains the increase of amplitude and also the occurrence of shadow zones close to the left boundary in Fig. 3a. In Fig. 5 we give a typical example of a trapped Rossby wave (group velocity or energy flux) ray. The energy propagates back and forth along a periodic (not closed) orbit. Such rays are ex-

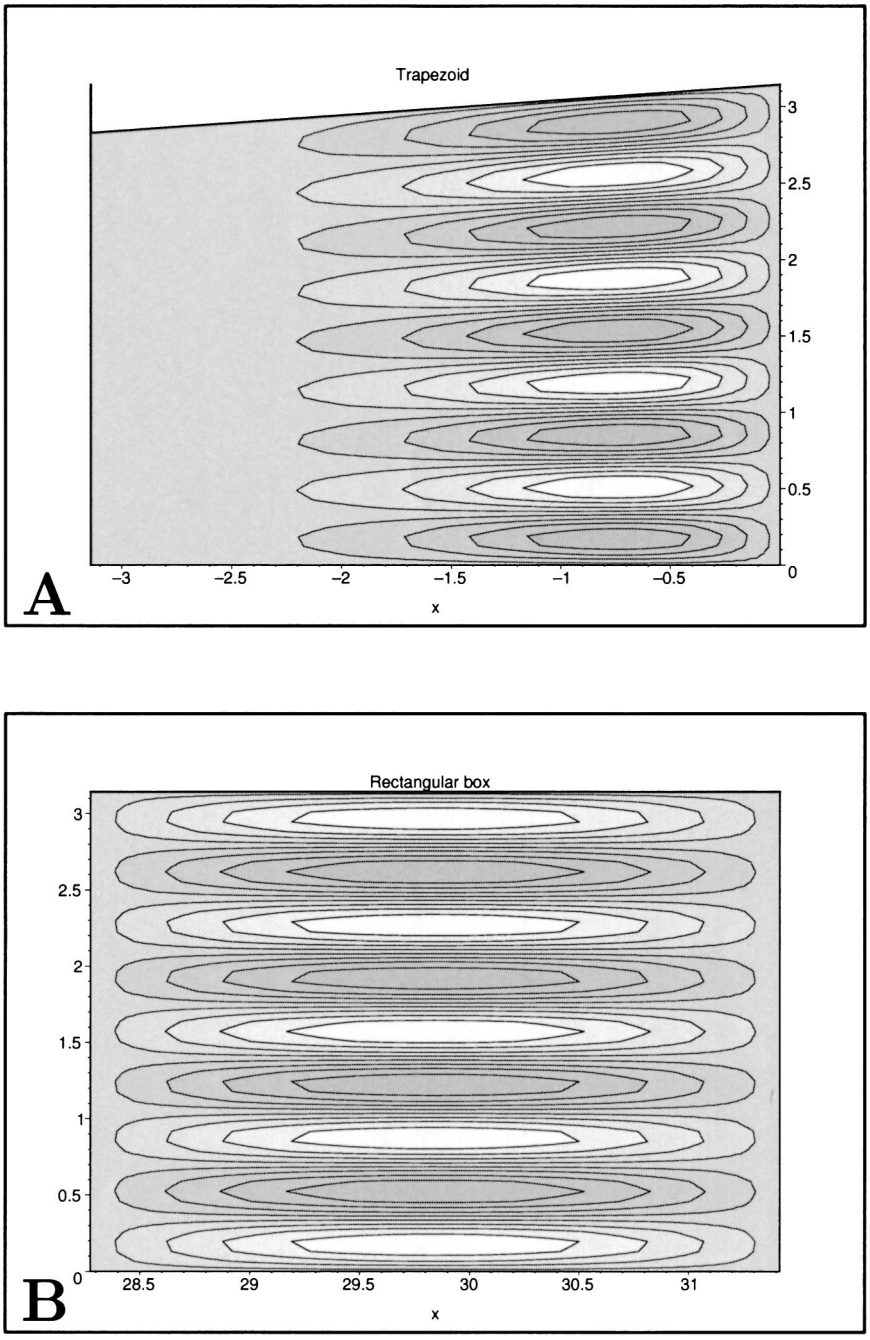

FIG. 3. Mode-1 solution of (a) (33) and (b) (23). Vertical wavenumber is $n = 9$, $\mu = 0.1$.

cluded if the half trapezoidal basin is approximated by a rectangle, and therefore the modes are erroneously always symmetric. On the other hand, asymmetric solutions appear to be captured well when the approximations (27), (33), and (35) are applied.[2]

Energy propagation of extratropical Rossby waves over slowly varying zonal topography has received increased attention recently, motivated by altimeter data analysis by Chelton and Schlax (1996). For example, Tailleux and McWilliams (2002) studied long Rossby

[2] Note that wave attractors discussed by Mass et al. (1997) for internal gravity waves do not exist for Rossby waves because of different reflection laws. When Rossby waves hit a boundary, the angle of reflection is equal to the angle of incidence. Such reflection excludes the existence of wave attractors.

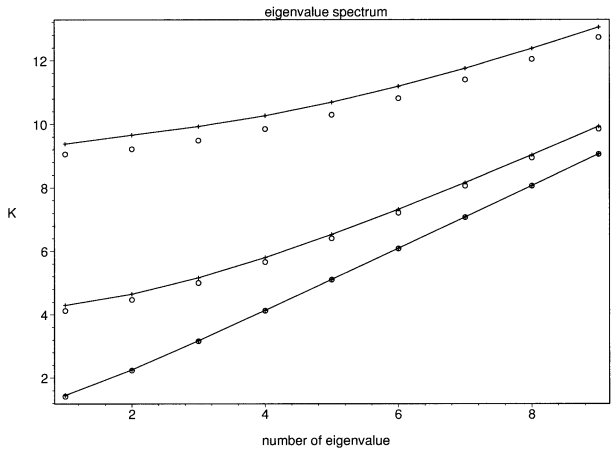

FIG. 4. The first nine eigenvalues computed by using (36) (crosses) and (23) (circles), where $n = 1$, 4, and 9. The slope corresponds to $\mu = 0.1$. The lowest curve corresponds to $n = 1$, the curve in the middle corresponds to $n = 4$, and the upper curve corresponds to $n = 9$. The crosses are connected by solid lines for clarity.

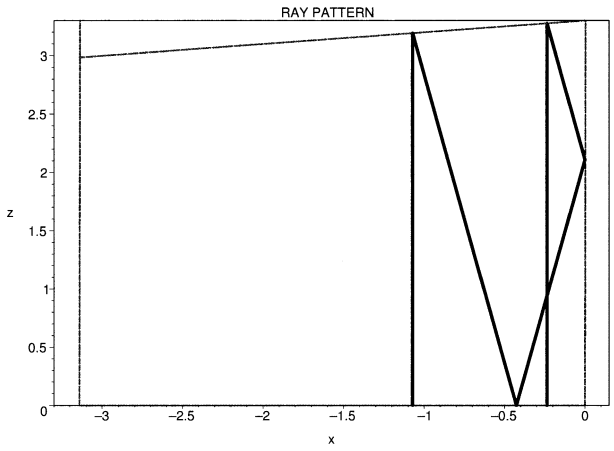

FIG. 5. Group velocity ray of a boundary trapped mode. Such rays are not possible when the actual basin shape is approximated by a square.

wave propagation by using a planetary geostrophic two-layer model without mean flow and friction but with a mountain ridge aligned in the north–south direction. We can create a comparable (but linearly stratified) situation using the baroclinic model by mirroring the basin shown in Fig. 1b along the vertical boundary at the shallow side. Removing then the vertical wall in the center we constructed a simple model with a ''midocean ridge,'' similar to the situation described by Tailleux and McWilliams. Because of the symmetry, the eigensolutions we described above are also solutions for the enlarged basin. Thus, we obtain the interesting result that high-energy (short wavelength) modes, excited at the lateral walls, cannot cross the ridge. This result might complement findings from planetary geostrophic models, which are not able to capture the synoptic-scale Rossby waves.

Rossby wave propagation in an ocean basin filled with a barotropic fluid is frequently discussed in the context of western boundary currents. Long waves propagate westward, are reflected at western boundaries, and turn to short waves. Some part of the energy accumulates at the western boundary; another part propagates eastward as short Rossby waves. Whether these short waves can be reflected at the eastern boundary depends on the basin's geometry. For example, for basins that become narrower to the east, reflection is not necessary to transform short eastward-propagating waves to longer waves, able to transport energy westward. As implied by this study, geometry-related turning might also be important. The same holds in the 2D baroclinic context for upslope propagating free waves. Low-frequency waves cannot reach the wall upslope, even for gentle topography. These effects are not captured using the linearized boundary condition.

Primeau (2002) recently studied Rossby wave dynamics in trapezoidal basins similar to the one shown in the upper panel of Fig. 1. However, the basins focused on by Primeau change width in the meridional direction. Moreover, Primeau focused on the effect of basin shape on resonant mode excitation using a 1½-layer dissipative model with a very small deformation radius (i.e., large F). In contrast, for the barotropic model, we focused here on the inviscid situation discussed, for example, by Flierl and not on ''long-wave basin modes'' discussed by Primeau or LaCasce and Pedlosky (2002).

Last, we mention that we have neglected mean circulation and viscosity in our analysis. Nevertheless, the solutions can be interpreted as ''unperturbed'' Rossby eigenmodes, useful as a starting point for stability analysis (Sheremet et al. 1997).

Considering the eigenvalue spectrum in Fig. 4 for the square and the half-trapezoidal basin, one might also expect very similar eigenfunctions. As we have shown, this is not the case. For many years it has been debated whether there is a one-to-one correspondence between boundary shape and eigenvalue spectrum (Kac 1966). It has surprisingly been shown that such a correspondence does not exist (Gordon et al. 1992). Here, in contrast, we have discussed an example in which boundary shape and eigenvalue spectra are very similar but eigenfunctions differ considerably.

Acknowledgments. We thank G. Terra and R. M. Samelson for useful discussions. The comments from two anonymous reviewers are acknowledged. Harlander was supported by the European Community in the form of a Marie Curie Fellowship (HPMF-CT-2000-00935).

REFERENCES

Abramowitz, M., and A. Stegun, 1965: *Handbook of Mathematical Functions.* Dover, 1046 pp.

Chelton, D. B., and M. G. Schlax, 1996: Global observations of oceanic Rossby waves. *Science,* **272,** 234–238.

Flierl, G. R., 1977: Simple applications of McWilliams' ''A note on a consistent quasigeostrophic model in a multiply connected domain.'' *Dyn. Atmos. Oceans,* **1,** 443–453.

Gerdes, R., and C. Wübber, 1991: Seasonal variability of the North Atlantic Ocean—A model intercomparison. *J. Phys. Oceanogr.,* **21,** 1300–1322.

Gordon, C., D. L. Webb, and S. Wolpert, 1992: One cannot hear the shape of a drum. *Bull. Amer. Math. Soc.,* **27,** 134–138.

Harlander, U., A. Gassmann, and W. Metz, 2001: Stationary Rossby wave propagation in a shear flow along a reflecting boundary. *Meteor. Atmos. Phys.,* **78,** 245–260.

——, H.-J. Schönfeldt, and W. Metz, 2000: Rossby waveguides in high-latitude shear flows with boundaries. *J. Geophys. Res.,* **105,** 17 063–17 078.

Holland, W. R., 1978: The role of mesoscale eddies in the general circulation of the ocean—Numerical experiments using a wind driven quasi-geostrophic model. *J. Phys. Oceanogr.,* **8,** 363–392.

Jensen, F. B., W. A. Kuperman, M. B. Porter, and H. Schmidt, 2000: *Computational Ocean Acoustics.* Springer-Verlag, 480 pp.

Kac, M., 1966: Can one hear the shape of a drum? *Amer. Math. Mon.,* **73B,** 1–23.

LaCasce, J. H., and J. Pedlosky, 2002: Baroclinic Rossby waves in irregular basins. *J. Phys. Oceanogr.,* **32,** 2828–2847.

LeBlond, P. H., and L. A. Mysak, 1978: *Waves in the Ocean.* Oceanography Series, Elsevier, 602 pp.

Maas, L. R. M., D. Benielli, J. Sommeria, and F.-P. A. Lam, 1997: Observation of an internal wave attractor in a confined, stable stratified fluid. *Nature,* **388,** 557–561.

McCartin, B. J., 2003: Eigenstructure of the equilateral triangle, Part I: The Dirichlet problem. *SIAM Rev.,* **45,** 267–287.

McWilliams, J. C., 1977: A note on a consistent quasigeostrophic model in a multiply connected domain. *Dyn. Atmos. Ocean,* **1,** 427–441.

Nedelec, J.-C., 2001: *Acoustic and Electromagnetic Equations.* Springer-Verlag, 316 pp.

Pedlosky, J., 1987: *Geophysical Fluid Dynamics.* 2d ed. Springer-Verlag, 710 pp.

Platzman, G. W., 1978: Normal modes of the World Ocean, Part I: Design of a finite-element barotropic model. *J. Phys. Oceanogr.,* **8,** 323–343.

Polyanin, A. D., 2002: *Handbook of Linear Partial Differential Equations for Engineers and Scientists.* CRC Press, 500 pp.

Primeau, F., 2002: Long Rossby wave basin-crossing time and the resonance of low-frequency basin modes. *J. Phys. Oceanogr.,* **32,** 2652–2665.

Rhines, P., 1970: Edge-, bottom-, and Rossby waves in a rotating stratified fluid. *Geophys. Fluid. Dyn.,* **1,** 273–302.

Sheremet, V. A., G. R. Ierley, and V. M. Kamenkovich, 1997: Eigenanalysis of the two-dimensional wind-driven ocean circulation problem. *J. Mar. Res.,* **55,** 57–92.

Stöckmann, H.-J., 1999: *Quantum Chaos.* Cambridge University Press, 368 pp.

Straub, D. N., 1994: Dispersive effects of zonally varying topography on quasi-geostrophic Rossby waves. *Geophys. Astrophys. Fluid Dyn.,* **75,** 107–130.

Tailleux, R., and J. C. McWilliams, 2002: Energy propagation of long extratropical Rossby waves over slowly varying zonal topography. *J. Fluid Mech.,* **473,** 295–319.

Zaitsev, O., R. Narevich, and R. E. Prange, 2001: Quasiclassical Born-Oppenheimer approximations. *Found. Phys.,* **31** (1), 7–26.